

Low-Reynolds number k - $\tilde{\epsilon}$ modelling of flows with transpiration

C.B. Hwang and C.A. Lin*

Department of Power Mechanical Engineering, National Tsing Hua University, Hsinchu, Taiwan 30043, Republic of China

SUMMARY

An improved low-Reynolds number k - $\tilde{\epsilon}$ model was adopted to predict the dynamic and thermal fields in flows with transpiration. The performance of the adopted model was first contrasted with the direct numerical simulation (DNS) data of channel flow with uniform wall injection and suction. The validity of the present model applied to flows with a high level of transpiration was further examined. To explore the model's performance in complex environments, the model was applied to simulate a transpired developing channel flow. By contrasting the predictions with DNS data and measurements, the results indicated that the present model reproduced correctly the deceleration and acceleration of the flow caused by the injection and suction from the permeable part of the wall. The turbulence structure of transpired flows was also well captured and the superior performance of the adopted model was reflected by the predicted correct level of ϵ with the maximum being located at both the injection and the suction walls. The predicted thermal field by the present model also compared favourably with the DNS data and measurements. Copyright © 2000 John Wiley & Sons, Ltd.

KEY WORDS: turbulence modelling; transpiration; dynamic field; turbulent field

1. INTRODUCTION

The adoption of wall transpiration as a flow control technique is frequently encountered in a variety of engineering applications. Injection from the permeable wall, for example, has been found to be an effective tool to produce film cooling for turbine blades exposed to a hot free stream. Because of the fluid injection into the mainstream, a thickened boundary layer is created, and consequently, the surface skin friction and hence the drag decreases. An elevated level of turbulent kinetic energy is also observed. In aeronautical applications, suction, on the other hand, is frequently used to delay the boundary layer separation and to inhibit the transition to turbulence. Even though the magnitude of the transpiration rate is often low

* Correspondence to: Department of Power Mechanical Engineering, National Tsing Hua University, Hsinchu, Taiwan 30043, Republic of China.

compared with the mainstream, it significantly changes the surface skin friction as well as the turbulence quantities near the wall.

With an aim to investigate the effects of wall transpiration on boundary layer development and heat transfer characteristics, many experiments [1–3] had been performed. Despite these efforts, the higher statistical quantities and the detailed near-wall flow structure of transpired flows are still lacking. This, however, is partly alleviated by the arrival of direct numerical simulations (DNS) of transpirational flows [4,5]. The simulated results not only reproduce the previously observed experimental findings of lower moments of the flow field, but they also provide the detailed budgets of the turbulent kinetic energy and its dissipation rate in the vicinity of the wall. The DNS data indicate that the magnitude of the maximum turbulence generation rate is larger on the injection wall and smaller on the suction wall compared with that on the wall without transpiration. Furthermore, the maximum dissipation rate is observed to be located on the transpired wall, as in the case of the non-transpired flows.

Although the DNS data can provide useful transpired flow information, the application of the DNS is still restricted to low-Reynolds number flows, which are rarely encountered in practical engineering applications. Besides, DNS is a computationally intensive scheme. Therefore, it is a common practice to adopt turbulence models to predict transpired flows [6–8].

Based on recent DNS data, a simplified form of a low-Reynolds number two-equation turbulence model was proposed [9]. Key features of the model are the adoption of the Taylor micro-scale in the damping function and the inclusions of the pressure diffusion terms in the k and ε equations. The inclusion of the pressure diffusion terms ensures the balance of the k and ε equations to be satisfied at the asymptotic state. However, the focus of the turbulence modelling was concentrated on non-permeable flows. In the present study, the proposed model is further applied to predict dynamic and thermal fields in flows with transpiration. The predictive performance of the model is assessed by comparisons with DNS data and measurements of transpired flows.

2. GOVERNING EQUATIONS

The Reynolds-averaged continuity, Navier–Stokes and temperature equations can be written as

$$\frac{\partial U_j}{\partial x_j} = 0, \quad (1)$$

$$\frac{\partial U_j U_i}{\partial x_j} = -\frac{1}{\rho} \frac{\partial P}{\partial x_i} + \frac{\partial}{\partial x_j} \left[\nu \left(\frac{\partial U_i}{\partial x_j} + \frac{\partial U_j}{\partial x_i} \right) - \overline{u_i u_j} \right], \quad (2)$$

$$\frac{\partial U_j T}{\partial x_j} = \frac{\partial}{\partial x_j} \left[\frac{\nu}{\sigma} \frac{\partial T}{\partial x_j} - \overline{u_j \theta} \right], \quad (3)$$

where ν and σ are the kinematic viscosity and Prandtl number respectively.

Within the framework of an eddy viscosity and adopting the Boussinesq approximation, the Reynolds stress and heat flux are approximated as

$$-\overline{u_i u_j} = \nu_t \left(\frac{\partial U_i}{\partial x_j} + \frac{\partial U_j}{\partial x_i} \right) - \frac{2}{3} \delta_{ij} k, \tag{4}$$

$$-\overline{u_j \theta} = \frac{\nu_t}{\sigma_t} \frac{\partial T}{\partial x_j}, \tag{5}$$

where ν_t and σ_t are the turbulent kinematic viscosity and Prandtl number respectively.

In the present application, the turbulence model adopted is the $k-\varepsilon$ model [10]. When applying the model towards the wall, the contribution of the molecular viscosity on the shear stress increases, and the standard high-Reynolds number turbulence must be modified to account for the diminishing effect of the near-wall turbulence levels. The construction of the low-Reynolds number model is the focus of the next section.

3. NEAR-WALL MODELLING

For the present approach, the turbulence is described by the eddy viscosity model that solves the transport equations for turbulent kinetic energy and turbulent dissipation rate.

The exact form of the transport equation for turbulent kinetic energy can be expressed as [11]

$$\frac{\partial U_j k}{\partial x_j} = \underbrace{\frac{\partial}{\partial x_j} \left(\nu \frac{\partial k}{\partial x_j} \right)}_{\mathcal{D}_k} - \underbrace{\frac{\partial}{\partial x_j} \left(\frac{1}{2} \overline{u_i u_i u_j} \right)}_{\mathcal{F}_k} - \underbrace{\frac{1}{\rho} \frac{\partial}{\partial x_j} (\overline{p u_j})}_{\Pi_k} - \underbrace{\overline{u_i u_j} \frac{\partial U_i}{\partial x_j}}_{\mathcal{P}_k} - \underbrace{\nu \frac{\partial u_i}{\partial x_j} \frac{\partial u_i}{\partial x_j}}_{\varepsilon}, \tag{6}$$

where \mathcal{D}_k , \mathcal{F}_k , Π_k , \mathcal{P}_k and ε are the laminar diffusion, the turbulent diffusion, the pressure diffusion, the turbulent production and the turbulent dissipation rate respectively.

The commonly adopted approach to model the turbulent diffusion term and the pressure diffusion term is to adopt a general gradient diffusion hypothesis, i.e.

$$\frac{\partial}{\partial x_j} \left[\frac{\nu_t}{\sigma_k} \frac{\partial k}{\partial x_j} \right] = - \underbrace{\frac{\partial}{\partial x_j} \left(\frac{1}{2} \overline{u_i u_i u_j} \right)}_{\mathcal{F}_k} - \underbrace{\frac{1}{\rho} \frac{\partial}{\partial x_j} (\overline{p u_j})}_{\Pi_k}, \tag{7}$$

where σ_k is the Prandtl number for k .

However, this modelling practice is only appropriate in the high-Reynolds number regime. Whereas in the near-wall region, the asymptotic behaviour of the turbulent diffusion term and the pressure diffusion term are different.

This can be verified by first examining the variations of the instantaneous velocity components with the distance from the wall, y . Following Launder [11] this can be expressed as

$$u = b_1 y + c_1 y^2 + d_1 y^3 + \dots, \tag{8}$$

$$v = c_2 y^2 + d_2 y^3 + \dots, \quad (9)$$

$$w = b_3 y + c_3 y^2 + d_3 y^3 + \dots, \quad (10)$$

where the coefficients b_i , c_i and d_i are functions of time whose mean value must be zero since $\overline{u_i} = 0$.

By inserting the y -dependent turbulent quantities into the k equation, it can be shown that, in the near-wall region, the following prevails:

$$\frac{\partial}{\partial x_j} \left[\frac{v_i}{\sigma_k} \frac{\partial k}{\partial x_j} \right] \approx \mathcal{O}(y^3), \quad (11)$$

$$\underbrace{-\frac{\partial}{\partial x_j} \left(\frac{1}{2} \overline{u_i u_i u_j} \right)}_{\mathcal{F}_k} \approx \mathcal{O}(y^3), \quad (12)$$

$$\underbrace{-\frac{1}{\rho} \frac{\partial}{\partial x_j} (\overline{p u_j})}_{\Pi_k} \approx \mathcal{O}(y). \quad (13)$$

If the modelling of the pressure diffusion term takes the form of Equation (7), the contribution of the pressure diffusion process will be absent in the near-wall region. This has a profound effect on the predicted near-wall turbulent dissipation rate level. Most models showed that the dissipation rate reached its maximum value somewhere inside the viscous sublayer. However, DNS data indicate that the maximum value of dissipation rate should be located at the wall itself. These, as argued by Kawamura [12], necessitate the inclusion of Π_k in the k equation, especially in the near-wall region. DNS indicates the influences of the pressure diffusion term rapidly decrease away from the wall, therefore Π_k is modelled as [12]

$$\Pi_k = -\frac{1}{2} v \frac{\partial}{\partial x_j} \left[\frac{k}{\varepsilon} \frac{\partial \hat{\varepsilon}}{\partial x_j} \right] \approx \mathcal{O}(y), \quad (14)$$

where $\hat{\varepsilon}$ is defined as

$$\hat{\varepsilon} = 2v \left(\frac{\partial \sqrt{k}}{\partial x_j} \right)^2.$$

It is also apparent that $\hat{\varepsilon}_w$ stands for the non-zero value of dissipation rate at the wall ε_w . Since $\hat{\varepsilon}$ approaches 0 at about $y^+ > 15$, this formulation confines the influence of Π_k to the wall region.

A similar approach can be applied to model the equation of the turbulent dissipation rate. There are currently two directions for solving the dissipation rate equation. The first one is the solution of the ε equation. The second approach is the decomposition of the dissipation rate into two parts, i.e. $\varepsilon = \tilde{\varepsilon} + \hat{\varepsilon}$, and adopting $\tilde{\varepsilon}$ as the dependent variable. Therefore, $\tilde{\varepsilon}$ is defined as the difference between ε [$= v(\partial u_i / \partial x_j)(\partial u_i / \partial x_j)$] and $\hat{\varepsilon}$ [$= 2v(\partial \sqrt{k} / \partial x_j)^2$]. The asymptotic behaviour of $\tilde{\varepsilon}$ is

$$\tilde{\varepsilon} = \varepsilon - \hat{\varepsilon} \approx \mathcal{O}(y^2). \tag{15}$$

As indicated previously, $\hat{\varepsilon}_w$ stands for the non-zero value of dissipation rate at the wall ε_w . Therefore, the advantage of this approach is that $\tilde{\varepsilon}$ reaches zero at the wall and $\tilde{\varepsilon}$ equals ε at about $y^+ > 15$, where $\hat{\varepsilon}$ approaches 0.

The commonly adopted form of the $\tilde{\varepsilon}$ equation can be expressed as [13]

$$\frac{\partial U_j \tilde{\varepsilon}}{\partial x_j} = \frac{\partial}{\partial x_j} \left(v \frac{\partial \tilde{\varepsilon}}{\partial x_j} \right) + \frac{\partial}{\partial x_j} \left(\frac{v_t}{\sigma_\varepsilon} \frac{\partial \tilde{\varepsilon}}{\partial x_j} \right) + C_{\varepsilon 1} f_1 \mathcal{P}_k \frac{\tilde{\varepsilon}}{k} - C_{\varepsilon 2} f_2 \frac{\tilde{\varepsilon}^2}{k} + \dots \tag{16}$$

In the vicinity of the wall, convection, turbulent diffusion and production go to zero very rapidly, and the asymptotic behaviour of the remaining term is

$$\frac{\partial}{\partial x_j} \left[v \frac{\partial \tilde{\varepsilon}}{\partial x_j} \right] \approx \mathcal{O}(1). \tag{17}$$

This necessitates the inclusion of the pressure diffusion to balance the equation and the form adopted is [9,11]

$$\Pi_{\tilde{\varepsilon}} = -v \frac{\partial}{\partial x_j} \left[\frac{\tilde{\varepsilon}}{k} \frac{\partial k}{\partial x_j} \right] \approx \mathcal{O}(1). \tag{18}$$

The idea of the inclusion of $\Pi_{\tilde{\varepsilon}}$ to balance the molecular diffusion at the wall was also adopted by Kawamura [12] and Chien [14], although with different formulations. However, only the present formulation mimics the diffusive nature of the pressure diffusion term. Furthermore, the proposed modelled $\Pi_{\tilde{\varepsilon}}$ also generates the extra source for ε in the buffer zone, completely replacing the commonly adopted function

$$v v_t \frac{\partial^2 U_i}{\partial x_j \partial x_k} \frac{\partial^2 U_i}{\partial x_j \partial x_k}.$$

Based on the above approach, an improved low-Reynolds number $k-\tilde{\varepsilon}$ model [9] was proposed and takes the form

$$v_t = 0.09 f_\mu(y_\lambda) \frac{k^2}{\tilde{\varepsilon}}, \tag{19}$$

$$\frac{\partial U_j k}{\partial x_j} = \frac{\partial}{\partial x_j} \left[v \frac{\partial k}{\partial x_j} \right] + \frac{\partial}{\partial x_j} \left[\frac{v_t}{\sigma_k} \frac{\partial k}{\partial x_j} \right] - \underbrace{\frac{1}{2} v \frac{\partial}{\partial x_j} \left[\frac{k}{\tilde{\varepsilon}} \frac{\partial \tilde{\varepsilon}}{\partial x_j} \right]}_{\Pi_k} - \overline{u_i u_j} \frac{\partial U_i}{\partial x_j} - (\tilde{\varepsilon} + \hat{\varepsilon}), \tag{20}$$

$$\frac{\partial U_j \tilde{\varepsilon}}{\partial x_j} = \frac{\partial}{\partial x_j} \left[v \frac{\partial \tilde{\varepsilon}}{\partial x_j} \right] + \frac{\partial}{\partial x_j} \left[\frac{v_t}{\sigma_\varepsilon} \frac{\partial \tilde{\varepsilon}}{\partial x_j} \right] - \underbrace{v \frac{\partial}{\partial x_j} \left[\frac{\tilde{\varepsilon}}{k} \frac{\partial k}{\partial x_j} \right]}_{\Pi_{\tilde{\varepsilon}}} - C_{\varepsilon 1} f_1 \overline{u_i u_j} \frac{\partial U_i}{\partial x_j} \frac{\tilde{\varepsilon}}{k} - C_{\varepsilon 2} f_2 \frac{\tilde{\varepsilon}^2}{k}, \tag{21}$$

where $y_\lambda = y/\sqrt{vk/\tilde{\epsilon}}$, $\sqrt{vk/\tilde{\epsilon}}$ is the Taylor micro-scale, and Π_k and $\Pi_{\tilde{\epsilon}}$ are pressure diffusion terms in the k and $\tilde{\epsilon}$ equations. The coefficients of the model are set to be

$$f_\mu = 1 - \exp(0.01y_\lambda - 0.08y_\lambda^3),$$

$$\sigma_k = 1.4 - 1.1 \exp\left(-\frac{y_\lambda}{10}\right),$$

$$\sigma_{\tilde{\epsilon}} = 1.3 - 1.0 \exp\left(-\frac{y_\lambda}{10}\right).$$

The adoption of y_λ avoids the obvious defect, i.e. the singularity occurring at the reattaching point by adopting $y^+ = U_\tau y/\nu$. The damping functions are chosen to retain the high-Reynolds number form away from the solid boundaries. The asymptotic values of the turbulent Prandtl number σ_k and $\sigma_{\tilde{\epsilon}}$ are chosen as 0.3 to obtain a sufficient dissipation rate in the vicinity of the wall. In the core region of the flow, $\sigma_k > \sigma_{\tilde{\epsilon}}$ is chosen to eliminate the common drawback that the turbulent diffusion of k overwhelms that of ϵ [15].

Table I. The constants and functions of various forms of $k-\tilde{\epsilon}$ models

Code	LS (1974) [13]	CH (1982) [14]	Present
Type	$k-\tilde{\epsilon}$	$k-\tilde{\epsilon}$	$k-\tilde{\epsilon}$
f_μ	$\exp\left[-3.4/\left(1 + \frac{Re_t}{50}\right)^2\right]$	$1 - \exp\left[-\frac{1.15y^+}{100}\right]$	$1 - \exp\left[-\frac{y_\lambda}{100} - \frac{8y_\lambda^3}{1000}\right]$
Π_k	0	0	$-\frac{1}{2}v \frac{\partial}{\partial x_j} \left[\frac{k}{\epsilon} \frac{\partial \tilde{\epsilon}}{\partial x_j} \right]$
C_μ	0.09	0.09	0.09
σ_k	1.0	1.0	$1.4 - 1.1 \exp(-y_\lambda/10)$
$\tilde{\epsilon}$	$2\nu(\partial\sqrt{k}/\partial y)^2$	$2\nu(k/y^2)$	$2\nu(\partial\sqrt{k}/\partial y)^2$
$\tilde{\epsilon}_w$	0	0	0
f_1	1	1	1
f_2	$1 - 0.3 \exp(-Re_t^2)$	$1 - 0.22 \exp[-(Re_t/6)^2]$	1
$\Pi_{\tilde{\epsilon}}$	0	$-2\nu(\tilde{\epsilon}/y^2) \exp(-0.5y^+)$	$-v \frac{\partial}{\partial x_j} \left[\frac{\tilde{\epsilon}}{k} \frac{\partial k}{\partial x_j} \right]$
E	$2\nu v_t \frac{\partial^2 U_i}{\partial x_j \partial x_k} \frac{\partial^2 U_i}{\partial x_j \partial x_k}$	0	0
$C_{\epsilon 1}$	1.44	1.35	1.44
$C_{\epsilon 2}$	1.92	1.8	1.92
$\sigma_{\tilde{\epsilon}}$	1.3	1.3	$1.3 - 1.0 \exp(-y_\lambda/10)$
	$Re_t = k^2/\nu\tilde{\epsilon}$	$Re_t = k^2/\nu\tilde{\epsilon}$	$Re_t = k^2/\nu\tilde{\epsilon}$
		$y^+ = yu_\tau/\nu$	$y_\lambda = y/\sqrt{(vk/\tilde{\epsilon})}$

The adopted form of f_μ reproduces correctly the asymptotic limit, i.e. $f_\mu \propto y$, and hence $-\overline{uw} \propto y^3$ towards the wall. The satisfaction of the asymptotic limit also guarantees the correct levels of ε with the maximum locating at the wall itself. This modification is important to properly mimic the turbulence levels and transfer rates as a wall is approached. Besides, the modelled pressure diffusion term $\Pi_{\tilde{\varepsilon}}$ also generates the extra source for $\tilde{\varepsilon}$ in the buffer zone, completely replacing the commonly adopted form of the extra term, $2\nu v_i(U_{i,jk})^2$ [13].

Here, the performance of the $k-\tilde{\varepsilon}$ models proposed by Launder and Sharma (LS) [13] and Chien (CH) [14], which were rated best in the review of Patel *et al.* [16] and Savill [17], are to be contrasted with the present model's predictions. The constants and functions adopted by the models are compiled in Table I.

4. NUMERICAL PROCEDURE

The present numerical procedure [18] solves discretized versions of all equations over a staggered finite volume arrangement. The principle of mass flux continuity is imposed indirectly via the solution of the pressure-correction equations according to the SIMPLE algorithm [19]. The flow property values at volume faces contained in the convective fluxes, which arise from the finite volume integration process, are approximated by the quadratic upstream-weighted interpolation scheme (QUICK) [20].

It was found that the use of the third-order approximation of the surface derivatives arising from the viscous and pressure diffusion processes is essential for reproducing the correct flow for near-wall asymptotic behaviour, by ensuring that the derivative is evaluated right at the surface. This can be expressed as

$$\int \frac{\partial}{\partial y} \left[v \frac{\partial k}{\partial y} \right] d\mathcal{V} = \left[v \frac{\partial k}{\partial y} \right]_N \Delta x_N - \left[v \frac{\partial k}{\partial y} \right]_S \Delta x_S + \dots, \tag{22}$$

$$\int -v \frac{\partial}{\partial y} \left[\frac{\tilde{\varepsilon}}{k} \frac{\partial k}{\partial y} \right] d\mathcal{V} = \left[-v \frac{\tilde{\varepsilon}}{k} \frac{\partial k}{\partial y} \right]_N \Delta x_N - \left[-v \frac{\tilde{\varepsilon}}{k} \frac{\partial k}{\partial y} \right]_S \Delta x_S + \dots, \tag{23}$$

where $\Delta\mathcal{V} = \Delta x \Delta y$, and the derivative $[\partial\phi/\partial y]_N$ must be located at the north surface. Applying a Taylor series expansion of the form

$$f(x) = f(a) + \frac{f'(a)}{1!} (x - a) + \frac{f''(a)}{2!} (x - a)^2 + \dots,$$

a surface derivative with third-order accuracy can be approximated as

$$\phi_j = \phi_{j+1} + \left(\frac{\partial\phi}{\partial y} \right)_{j+1} (y_j - y_{j+1}) + \frac{1}{2} \left(\frac{\partial^2\phi}{\partial y^2} \right)_{j+1} (y_j - y_{j+1})^2 + \mathcal{O}(y^3), \tag{24}$$

$$\phi_{j-1} = \phi_{j+1} + \left(\frac{\partial\phi}{\partial y} \right)_{j+1} (y_{j-1} - y_{j+1}) + \frac{1}{2} \left(\frac{\partial^2\phi}{\partial y^2} \right)_{j+1} (y_{j-1} - y_{j+1})^2 + \mathcal{O}(y^3) \tag{25}$$

and

$$\left(\frac{\partial\phi}{\partial y}\right)_{j+1} = \frac{(y_{j-1} - y_{j+1})^2\phi_j - (y_j - y_{j+1})^2\phi_{j-1} - [(y_{j-1} - y_{j+1})^2 - (y_j - y_{j+1})^2]\phi_{j+1}}{(y_{j-1} - y_{j+1})(y_j - y_{j+1})(y_{j-1} - y_j)}, \quad (26)$$

where j and $j+1$ are the wall proximity and wall surface nodes respectively, and y is the location of the dependent variable.

The computed solution is assumed to have converged to its steady state when the magnitude of the absolute residual sources of mass and momentum, normalized by the respective inlet fluxes, falls below 0.01%.

5. RESULTS AND DISCUSSIONS

5.1. Channel flow with a uniform transpiration dynamic field

The performance of the proposed model is first contrasted with the DNS data of a channel flow with uniform wall injection and suction [5]. The schematic picture of the flow is shown in Figure 1. The Reynolds number Re_τ , based on the wall friction velocity U_τ and the channel half-width δ , was set at 150, where U_τ is the averaged wall shear stress on the two walls. The mass flux ratios on both walls were $F = v_0/U_m = 0.00344$, in which v_0 is the wall-normal velocity and U_m is the axial bulk mean velocity.

Grid densities of sizes 60 and 100 in the direction normal to the wall were used to check the grid independence. Preliminary results indicated that the two meshes produced nearly identical results, therefore, the 60 grid was used for all subsequent calculations. To ensure the resolution of the viscous sublayer, the first grid node near the wall was placed at $y_+ \approx 0.1$.

The influence of the wall transpiration on the flow can be seen by the asymmetric axial velocity distribution across the channel, shown in Figure 2. For comparisons, the $Re_\tau = 150$ DNS data [21] in a fully developed channel flow without wall transpiration are also shown in

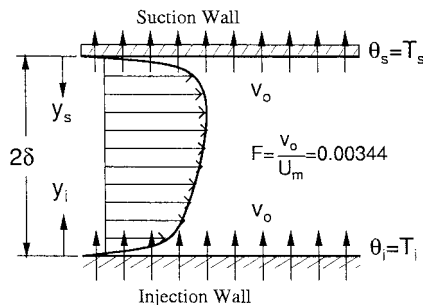


Figure 1. Geometry of turbulent plane flow with uniform wall transpiration.

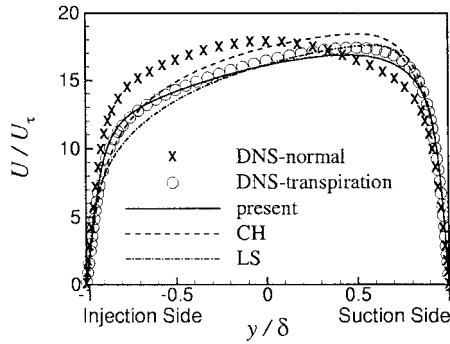


Figure 2. Mean velocity profile.

the figure. It can be clearly seen that the location of the maximum axial velocity is observed to shift towards the suction side, in which the near-wall velocity is accelerated due to the suction flux. The log-law plots on both of the walls are shown in Figures 3 and 4, and a marked different distribution to that without wall transpiration is observed. Referring to Figure 3, an improved prediction by the adopted model is observed in the injection region, and the predicted profile agrees well with the DNS distribution.

Regarding the Reynolds stress, all the models can deliver reasonable predictions, as shown in Figure 5. Further examination of the performances of the models can be directed to the k^+ distributions shown in Figure 6, in the near-wall region. In strong contrast to the shear stress distributions, not all the model can accurately predict the distributions of the turbulent kinetic energy. While the LS model underpredicted the peak value, the best result is predicted by the proposed model. By contrasting the results without wall transpiration, the effects of the presence of injection and suction on the wall are observed to promote and inhibit turbulence generation respectively.

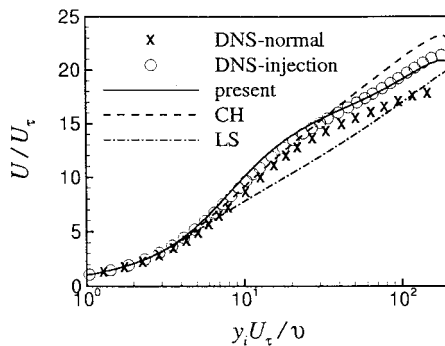


Figure 3. Mean velocity plotted from the injection wall.

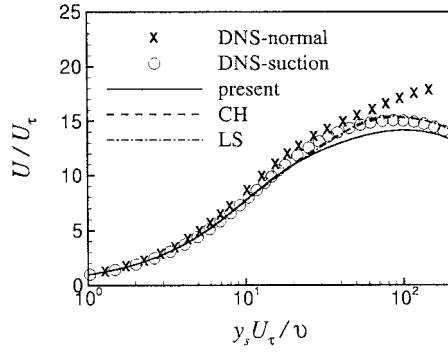


Figure 4. Mean velocity plotted from the suction wall.

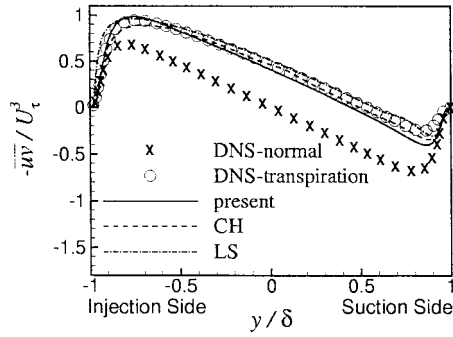


Figure 5. Shear stress distribution.

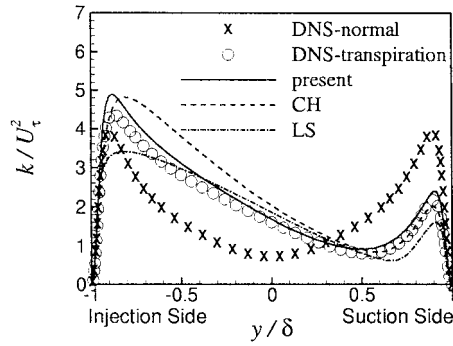


Figure 6. Turbulent kinetic energy distribution.

The effect of the inclusion of pressure diffusion terms as indicated earlier, is best exemplified by observing the ϵ^+ distributions in the near-wall region, shown in Figure 7. Despite the presence of wall transpiration, the DNS indicates that the location of the maximum dissipation rate is right on the wall, as in the case without wall transpiration. The present model shows the correct level of ϵ with the maximum located at the wall and, in strong contrast, the CH and LS models indicate a misplaced local maxima.

The overall performance of the model is evaluated by examining the predicted turbulence kinetic energy budgets in the near-wall region, shown in Figures 8–10, where Figure 8 shows the results without wall transpiration. By contrasting with the DNS data, the quality of the present model predictions can be further ascertained. The k -budget is in general dominated by production and dissipation processes away from the wall. In the vicinity of the wall, the dissipation rate balances the viscous diffusion process. The effects of the presence of injection

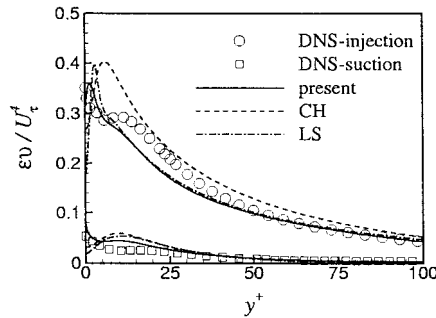


Figure 7. Turbulent dissipation rate ϵ^+ distributions.

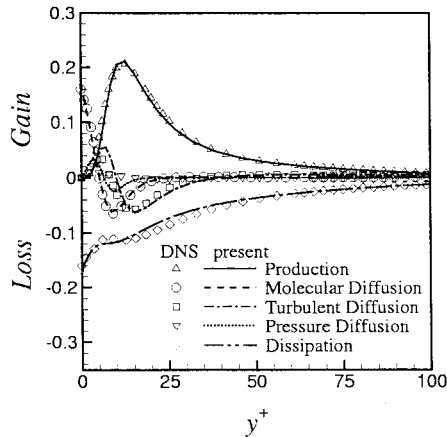


Figure 8. Budget of turbulent kinetic energy without transpiration.

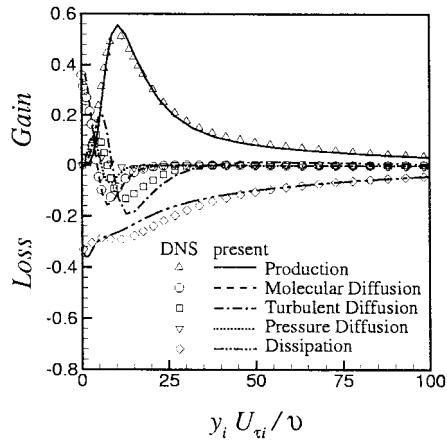


Figure 9. Budget of turbulent kinetic energy in the injection region.

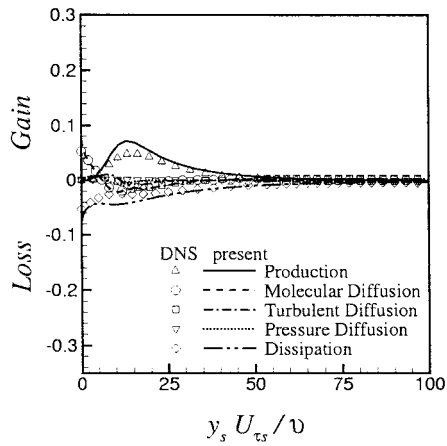


Figure 10. Budget of turbulent kinetic energy in the suction region.

and suction at the wall can be observed to promote and inhibit turbulence generation, respectively. The maximum generation rate on the injection and suction walls is about three times and a quarter to the maximum one without wall transpiration.

To explore the model's performance in the high-Reynolds number flows, the predicted skin friction coefficients with different levels of wall transpiration are contrasted with the large eddy simulation (LES) data [22] and measurements [23,24]. Three transpiration rates were used in this study, and the flow conditions adopted are listed in Table II.

Table II. The operating conditions for transpired flows

LES data (exit $Re_m = 56\,840$)				
	Blowing		Suction	
	Present	LES [22]	Present	LES [22]
$F = v_0/U_{\max}$	0.00375	0.004	-0.00375	-0.004
$b_f = 2F/c_{f,NT}$	2.071	2.030	-2.071	-2.030
LES data (exit $Re_m = 23\,853$)				
	Blowing		Suction	
	Present	LES [22]	Present	LES [22]
$F = v_0/U_{\max}$	0.002	0.00188	-0.002	-0.00188
$b_f = 2F/c_{f,NT}$	0.9	0.85	-0.9	-0.85
DNS data (Exit $Re_m = 4446$)				
	Blowing		Suction	
	Present	DNS [5]	Present	DNS [5]
$F = v_0/U_{\max}$	0.003	0.003	-0.003	-0.003
$b_f = 2F/c_{f,NT}$	0.899	0.9	-0.92	-0.9

The present fully developed channel flows are compared with the constant pressure case measurements [23,24], i.e. the accelerating parameter $K = (v/U_{\infty}^2)(dU_{\infty}/dx)$ is zero. This is motivated by the work of Piomelli *et al.* [22], which indicated that the physical phenomena encountered in a fully developed transpired channel are sufficiently similar to those in a constant pressure boundary layer to allow comparison with the constant pressure boundary layer results. Therefore, the adopted measurements are with constant free stream velocity. The Reynolds number (Re_{δ}) based on the momentum thickness ranges from 667 to 3151, and the mass flux ratio (F) ranges from 0.008 to -0.002 .

The predicted friction coefficient normalized with the friction coefficient without wall transpiration is shown in Figure 11, where the solid line is based on the equation proposed by Simpson *et al.* [25]. The dashed line is the direct extension of the Simpson *et al.*'s equation to the suction side. It can be clearly seen that the predicted skin friction coefficient of the present model agrees well with the LES and experimental data, and this indicates the validity of the present model in applying to flows with high level of transpiration.

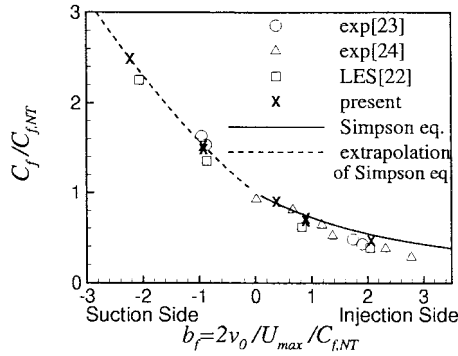


Figure 11. Ratio of friction coefficient to friction coefficient without transpiration.

5.2. Channel flow with a uniform transpiration thermal field

In this section, the focus here is on the predictive capability of the model to a thermal field with constant wall temperature within the aforementioned channel flow with wall transpiration [5]. Traditionally, the thermal diffusivity is assumed to be $\alpha_t = \nu_t/Pr_t$, and the commonly adopted value of Pr_t is 0.9 [10]. However, the recent DNS data [26,27] indicate that the wall value of the turbulent Prandtl number is about 1.1 for normal and large viscous Prandtl number fluids. Preliminary predictions with two different Pr_t indicate marginal difference, though a prediction with $Pr_t = 1.1$ shows more accurate turbulent heat fluxes.

The predicted normalized temperature and turbulent heat flux are shown in Figures 12 and 13, together with DNS data [5]. It can be observed that the assumption of constant turbulent Prandtl number could capture the essential characteristics of the thermal field. Referring to Figures 13 and 14, it can be clearly seen that the present model shows better results than the other two models do. This might be attributed to the correct dynamic field predicted.

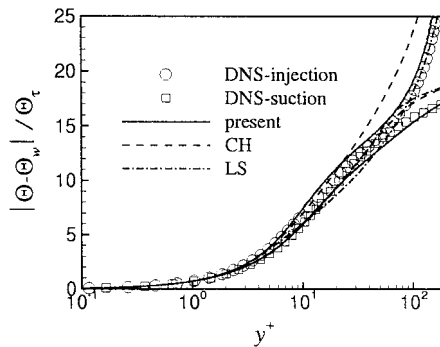


Figure 12. Mean temperature profile for $Pr = 1.1$.

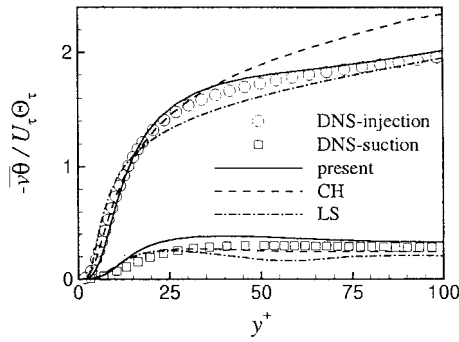


Figure 13. Turbulent heat flux for $Pr = 1.1$.

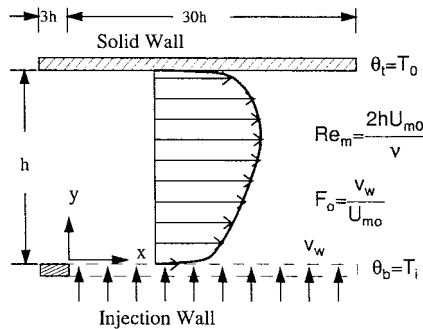


Figure 14. Geometry of duct flow with fluid injection from wall.

5.3. Developing channel flow with uniform injection

To further explore the model’s performance in complex environments, the model is applied to simulate flow in a two-dimensional duct with fluid injection from a permeable part of the wall. Measurements [7] of the flow quantities as well as wall heat transfer characteristics are available to evaluate the model’s performance. The geometry of the duct is shown in Figure 14. Flows with three Reynolds number, $Re_m (= 2hU_{m0}/\nu) = 6700, 9030, \text{ and } 18500$, were investigated, where h is the channel height, U_{m0} is the average inlet streamwise velocity and ν is the kinematic viscosity. Different levels of injection from the permeable wall were also investigated and the injection rate is defined as $F_0 = v_w/U_{m0}$, where v_w is the injection velocity. Based on a previous investigation of non-permeable flow [9] and the results from the previous section, a grid of size 100×60 , which was non-uniform in both the x - and y -direction, was adopted. The first near-wall grid node was placed at $y^+ \leq 0.5$.

Attention here is drawn to the predictions by the present model, and the predictions by the CH model are also shown for comparisons. The influences of the injection on the flows at

different Reynolds numbers and injection rates can be seen from the streamwise velocity, shown in Figures 15–17. Due to the presence of the injection from the bottom wall, the location of the maximum velocity has been shifted upward. An excessive deceleration of the streamwise velocity near the permeable wall was predicted by the CH model compared with the measurements, and the simulation by the present model shows the correct level of flow development.

Finally, attention is directed to the heat transfer predictions at different levels of the wall injection rates. It can be clearly seen that the elevated level of wall transpiration causes the reduction of the Nusselt number (Figure 18). Although both the present and CH models can reproduce this phenomenon, the reduction of Nu predicted by the CH model is excessive compared with the measurements.

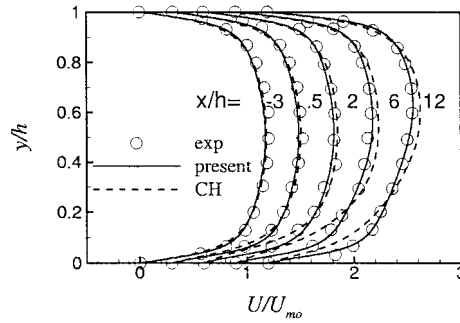


Figure 15. Axial velocity distribution— $Re_m = 6700$, $F_0 = 0.0087$.

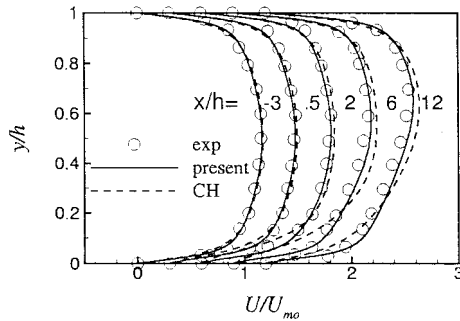


Figure 16. Axial velocity distribution— $Re_m = 9030$, $F_0 = 0.01$.

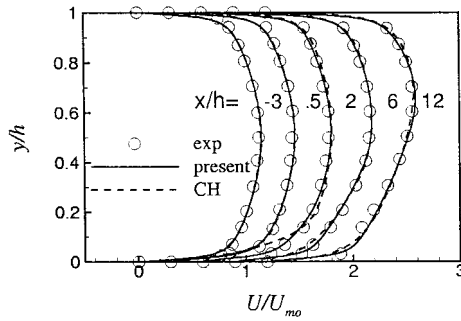


Figure 17. Axial velocity distribution— $Re_m = 18500$, $F_0 = 0.015$.

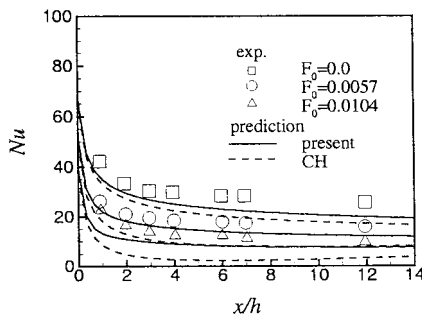


Figure 18. Nusselt number distribution— $Re_m = 6000$.

6. CONCLUSION

Dynamic and thermal fields within flows with wall transpiration were predicted by an improved low-Reynolds number $k-\tilde{\epsilon}$ model. The performance of the proposed model was first contrasted with the DNS data of a channel flow with uniform wall injection and suction. Despite the presence of wall transpiration, the DNS data indicated that the location of the maximum dissipation rate is right on the wall, as in the case without wall transpiration. The superior performance of the adopted model was reflected by the predicted correct level of ϵ with the maximum being located at the wall and, in strong contrast, the CH and LS models indicated misplaced local maxima. By comparing the predicted skin friction coefficient with the DNS and LES data, the validity of the present model being applied to flows with a high level of transpiration was ascertained. The predicted thermal field by the present model also compared favourably with the DNS data. The model was further applied to simulate a transpired developing channel flow. By contrasting the predicted results with measurements, the results indicated that the present model reproduced correctly the deceleration of the flow caused by the wall injection and the near-wall heat transfer behaviour.

ACKNOWLEDGMENTS

This research work was supported by the National Science Council of Taiwan under grant NSC85-2212-E-007-057 and the computational facilities were provided by the National Centre for High-Performance Computing of Taiwan which the authors gratefully acknowledge.

APPENDIX A. NOMENCLATURE

b_f	dimensionless blowing parameter
C_p	specific heat at constant pressure
$C_\mu, C_{\varepsilon 1}, C_{\varepsilon 2}$	coefficients in turbulence model
C_f	skin friction coefficient
E	source term in turbulence model
f_μ	damping function in turbulence model
h	channel height
k	turbulent kinetic energy, $\overline{u_i u_i}/2$
k^+	normalized turbulent kinetic energy, k/U_τ^2
K	accelerating parameter
Nu	Nusselt number
P	mean pressure
Pr, Pr_t	molecular and turbulent Prandtl numbers
q_w	wall heat flux
Re_m	Reynolds number based on bulk mean velocity, $U_m h/\nu$
Re_δ	Reynolds number based on momentum thickness, $U_\infty \delta/\nu$
Re_τ	Reynolds number based on U_τ , $U_\tau h/\nu$
Re_t	turbulent Reynolds number, $k^2/\nu \tilde{\varepsilon}$
u	fluctuation velocity
$u_i u_j$	Reynolds stress
$u_j \theta$	turbulent heat flux
U_i	mean velocity component in x_i -direction
U_m, U_{m0}	the axial bulk mean velocity
U_{\max}	the maximum of axial mean velocity
U_∞	free stream velocity
U_τ	friction velocity, $\sqrt{\tau_w/\rho}$
v_0, v_w	wall-normal velocity
x, y	co-ordinate in streamwise and wall-normal directions
y^+	normalized y co-ordinate, yU_τ/ν
y_i, y_s	distance from the injection or suction wall surfaces
y_λ	Taylor micro-scale, $\sqrt{\nu k/\tilde{\varepsilon}}$
x_i	Cartesian co-ordinate in i -direction
<i>Greek letters</i>	
α, α_t	thermal and turbulent heat diffusivities
δ	channel half width or momentum thickness

δ_{ij}	Kronecker delta
ε	total turbulent dissipation rate, $v(\overline{\partial u_i / \partial x_j})^2$
ε^+	normalized dissipation rate, $\varepsilon v / U_\tau^4$
$\hat{\varepsilon}$	'wall' dissipation, $2v(\partial \sqrt{k} / \partial x_j)^2$
$\tilde{\varepsilon}$	isotropic dissipation rate, $\varepsilon - \hat{\varepsilon}$
μ	molecular viscosity
ν, ν_t	kinematic and eddy viscosities
θ	fluctuating temperature
ρ	mean density
σ	Prandtl number
$\sigma_k, \sigma_{\tilde{\varepsilon}}$	turbulence model constants for diffusion of $k, \tilde{\varepsilon}$
τ_w	wall shear stress
$\Pi_k, \Pi_{\tilde{\varepsilon}}$	pressure diffusion rate of $k, \tilde{\varepsilon}$
Θ	mean temperature
Θ_τ	friction temperature, $q_w / \rho C_p U_\tau$

Subscripts

i, j, k	tensorial direction indices
i, s	at injection or suction wall surfaces
k	kinetic energy equation
m	bulk mean
$0, NT$	without transpiration
t	turbulent
w	at the wall
ε	in dissipation equation
λ	based on Taylor micro-scale
μ	in eddy viscosity formulation
τ	based on U_τ

Superscripts

+	dimensionless quantities
---	--------------------------

Mathematical symbol

$(\overline{\quad})$	time-averaged value
----------------------	---------------------

REFERENCES

1. M. Schildknecht, J.A. Miller and G.E.A. Meier, 'The influence of suction on the structure of turbulence in fully developed pipe flow', *J. Fluid Mech.*, **90**, 67–107 (1979).
2. M. Sano, 'Turbulent structure in channel flow with injection', *Trans. JSME B*, **60**, 2377–2382 (1994).
3. R.A. Antonia, Y. Zhu and M. Sokolov, 'Effect of concentrated wall suction on a turbulent boundary layer', *Phys. Fluids*, **7**, 2465–2474 (1995).
4. P. Mariani, P. Spalart and W. Kollmann, 'Direct simulation of a turbulent boundary layer with suction', in R.M.C. So, C.G. Speziale and B.E. Launder (eds.), *Near-Wall Turbulent Flows*, Elsevier, Amsterdam, 1993, pp. 347–356.

5. Y. Sumitani and N. Kasagi, 'Direct numerical simulation of turbulent transport with uniform wall injection and suction', *AIAA J.*, **33**, 1220–1228 (1995).
6. R.M.C. So and G.J. Yoo, 'Low Reynolds number modeling of turbulent flows with and without wall transpiration', *AIAA J.*, **25**, 1556–1564 (1987).
7. A.K. Abdel-Rahman, Y. Hagiwara and K. Suzuki, 'Turbulent flow and heat transport in a duct with fluid injection from wall', *Proc. 9th Symp. on Turbulent Shear Flow*, Kyoto, Japan, 1993, pp. 18.4.1–18.4.6.
8. D. Sofialidis and P.A. Prinos, 'Wall suction effects on the structure of fully developed turbulent pipe flow', *ASME J. Fluids Eng.*, **118**, 33–38 (1996).
9. C.B. Hwang and C.A. Lin, 'Improved low-Reynolds number $k-\tilde{\epsilon}$ model based on direct numerical simulation data', *AIAA J.*, **36**, 38–43 (1998).
10. W.P. Jones and B.E. Launder, 'The calculation of low-Reynolds number phenomena with a two-equation model of turbulence', *Int. J. Heat Mass Transf.*, **16**, 1119–1130 (1973).
11. B.E. Launder, 'Low-Reynolds number turbulence near walls', *Report TFD/86/4*, Department of Mechanical Engineering, University of Manchester Institute of Science and Technology, Manchester, UK, February 1984.
12. H. Kawamura, 'A $k-\epsilon-v^2$ model with special relevance to the near wall turbulence', *Proc. 8th Symp. on Turbulent Shear Flow*, Munich, Germany, 1991, pp. 26.4.1–26.4.6.
13. B.E. Launder and B.I. Sharma, 'Application of the energy dissipation model of turbulence to the calculation of flow near a spinning disc', *Lett. Heat Mass Transf.*, **1**, 131–138 (1974).
14. K.Y. Chien, 'Predictions of channel and boundary layer flows with a low-Reynolds number turbulence model', *AIAA J.*, **20**, 33–38 (1982).
15. T. Nagano and M. Tagawa, 'An improved $k-\epsilon$ model for boundary layer flows', *ASME J. Fluids Eng.*, **112**, 33–39 (1990).
16. V.C. Patel, W. Rodi and G. Scheuerer, 'Turbulence models for near-wall and low-Reynolds number flows: a review', *AIAA J.*, **23**, 1308–1319 (1985).
17. A.M. Savil, 'Some recent progress in the turbulence modelling of by-pass transition', in R.M.C. So, C.G. Speziale and B.E. Launder (eds.), *Near-Wall Turbulent Flows*, Elsevier, Amsterdam, 1993, pp. 829–848.
18. C.A. Lin and M.A. Leschziner, 'Three-dimensional computation of transient interaction between radially injected jet and swirling cross-flow using second-moment closure', *Comput. Fluid Dyn. J.*, **1**, 423–432 (1993).
19. S.V. Patankar, *Numerical Heat Transfer and Fluid Flow*, Hemisphere Publishing, New York, 1980.
20. B.P. Leonard, 'A stable and accurate convective modelling procedure based on quadratic upstream interpolation', *Comput. Methods Appl. Mech. Eng.*, **19**, 59–98 (1979).
21. A. Kuroda, N. Kasagi and M. Hirata, 'Direct numerical simulation of turbulent plane Couette–Poiseuille flows: effect of mean shear on the near wall turbulence structure', *Proc. 9th Symp. on Turbulent Shear Flow*, Kyoto, Japan, 1993, pp. 8.4.1–8.4.6.
22. U. Piomelli, P. Moin and J. Ferziger, 'Large eddy simulation of the flow in a transpired channel', *J. Thermophys.*, **5**, 124–128 (1991).
23. H.L. Julien, W.M. Kays and R.J. Moffat, 'Experimental hydrodynamics of the accelerated turbulent boundary layer with and without mass injection', *ASME J. Heat Transf.*, **93**, 373–379 (1971).
24. P.S. Anderson, W.M. Kays and R.J. Moffat, 'Experimental results for the transpired turbulent boundary layer in an adverse pressure gradient', *J. Fluid Mech.*, **69**, 353–375 (1975).
25. R.L. Simpson, R.J. Moffat and W.M. Kays, 'The turbulent boundary layer on a porous plate: experimental skin friction with variable injection and suction', *Int. J. Heat Mass Transf.*, **12**, 771–789 (1969).
26. R.A. Antonia and J. Kim, 'Turbulent Prandtl number in the near-wall region of a turbulent channel flow', *Int. J. Heat Mass Transf.*, **34**, 1905–1908 (1991).
27. J. Kim and P. Moin, 'Transport of passive scalars in a turbulent channel flow', in *Turbulent Shear Flow*, vol. 6, Springer, Berlin, 1989, pp. 85–96.